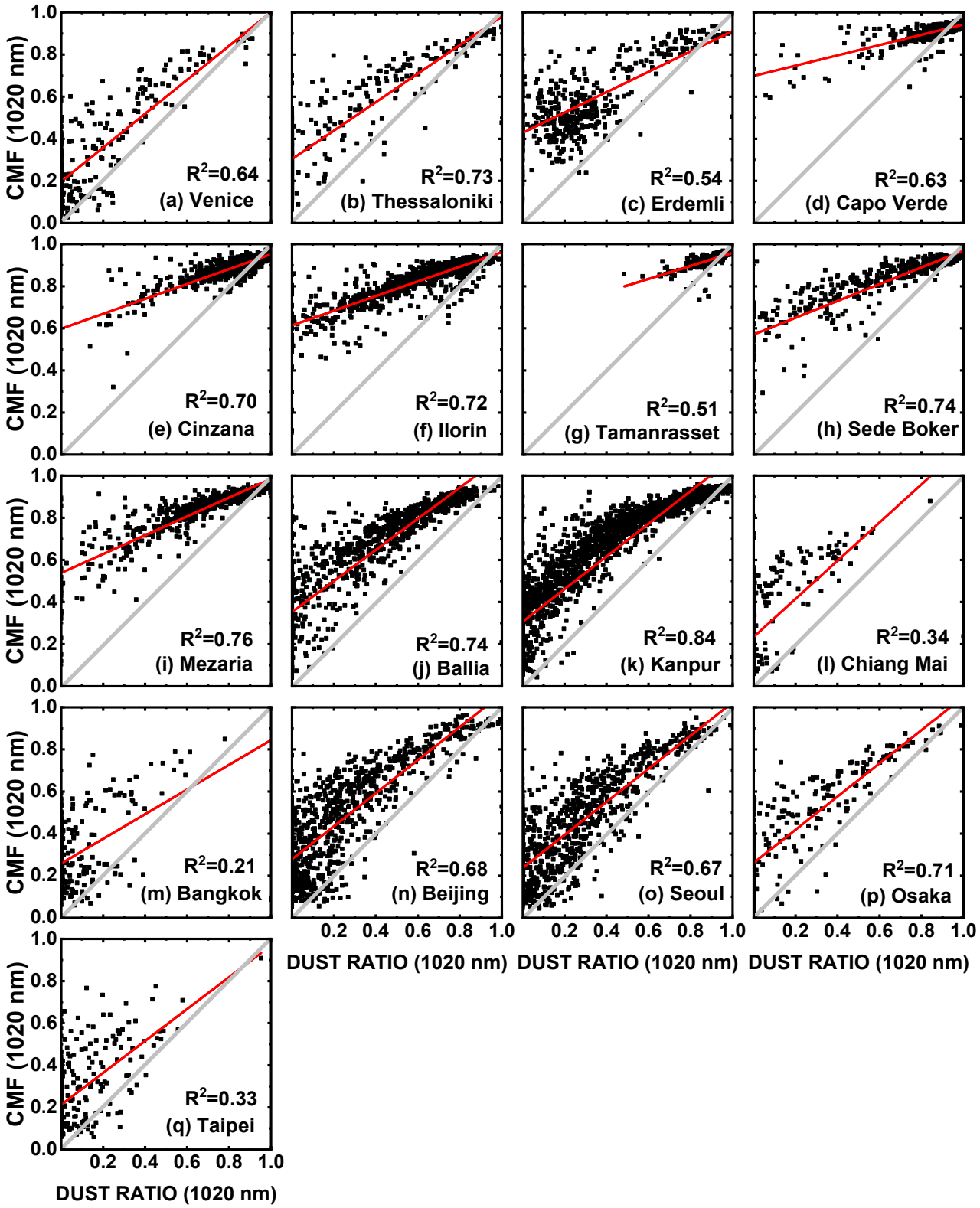

Figure S1. Correlation coefficient, R^2 between dust ratio (R_D) at wavelength 1020 nm and coarse mode fraction of the particle size distributions for each of the AERONET sites.

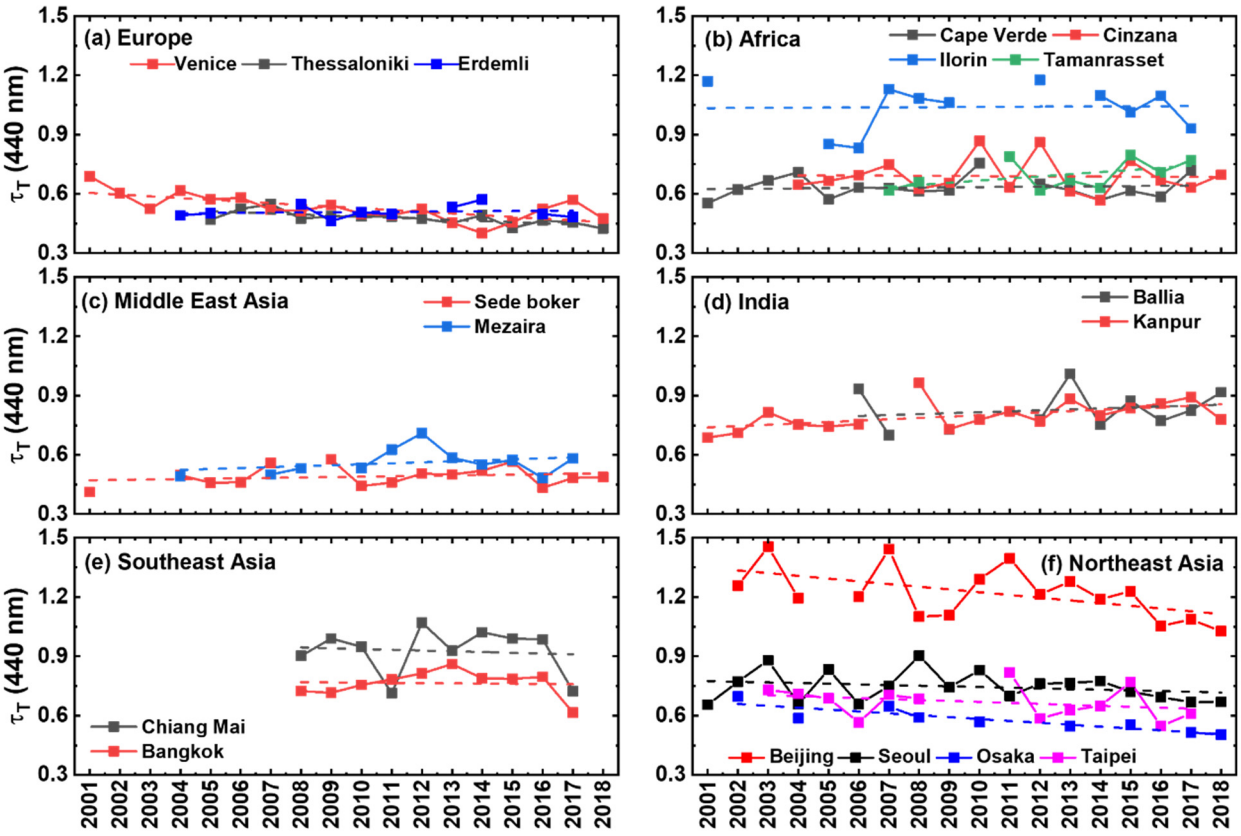

Figure S2. Annual trend of total AOD (τ_T) at wavelength 440 nm for the 17 AERONET sites for the timeframe from 2001–2018. The dashed lines show ordinary least square regression lines.

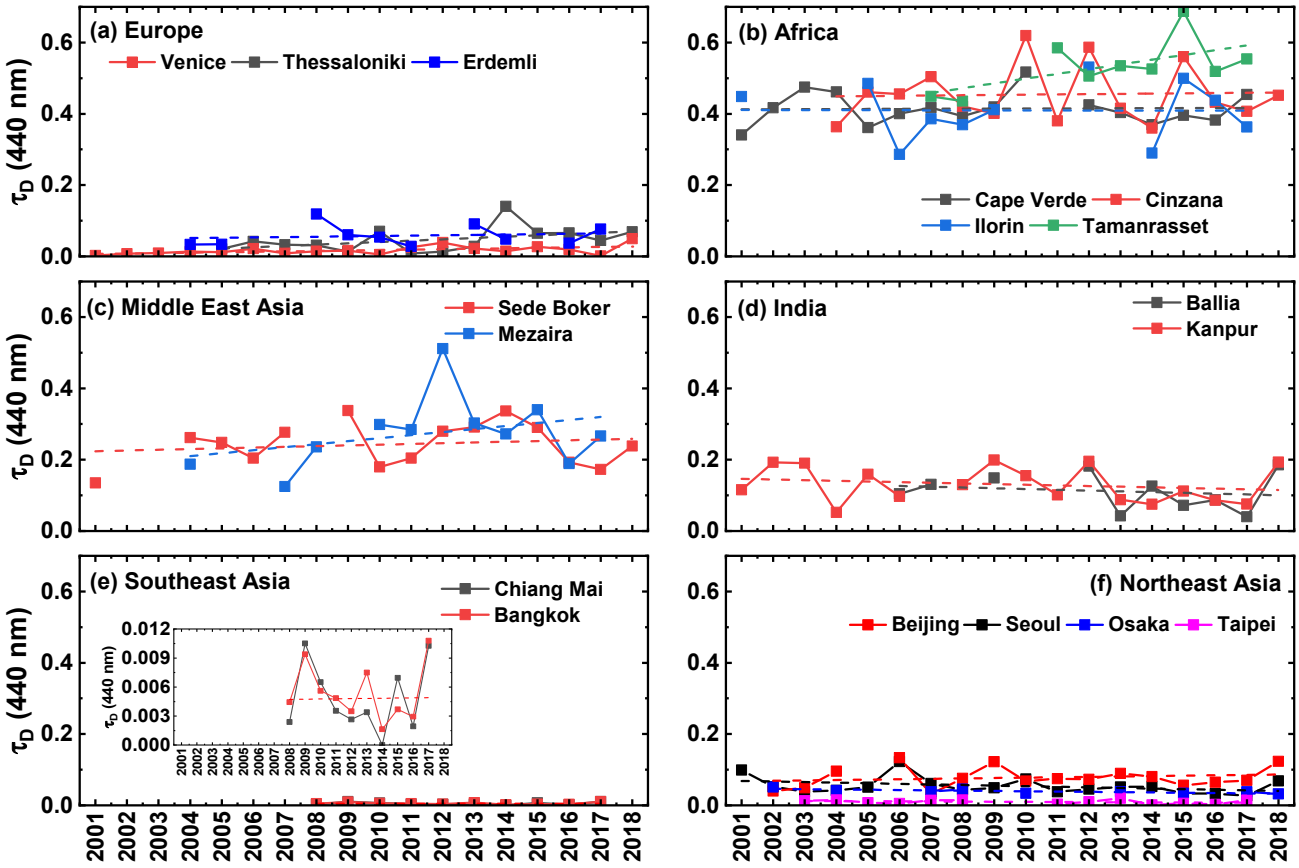

Figure S3. Annual trend of dust-only AOD (τ_D) at wavelength 440 nm for the 17 AERONET sites for the timeframe from 2001–2018. The dashed lines show ordinary least square regression lines.

Figure S4. Annual trend of coarse-mode pollution AOD (τ_{PC}) at wavelength 440 nm for the 17 AERONET sites for the timeframe from 2001–2018. The dashed lines show ordinary least square regression lines.

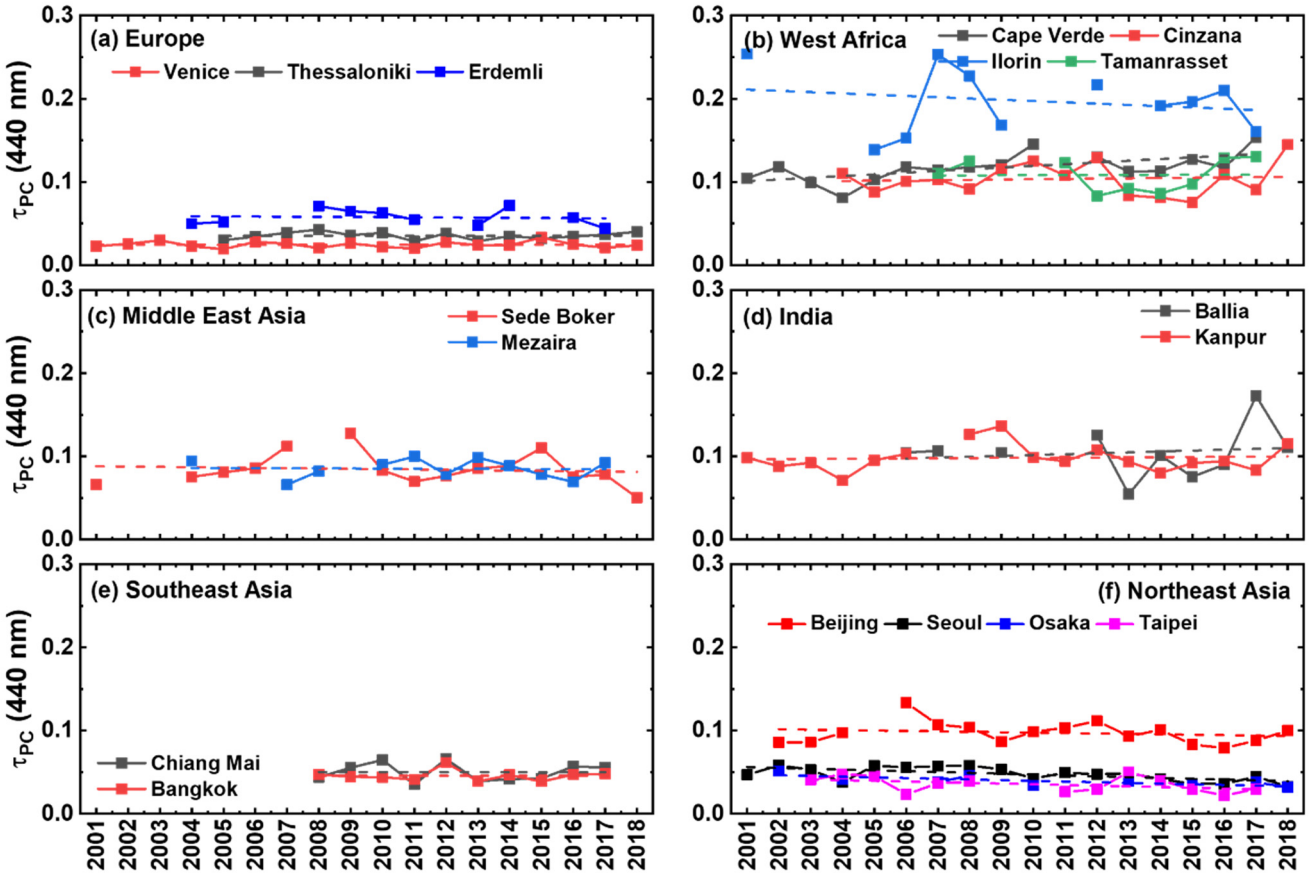

Figure S5. Annual trend of fine-mode pollution AOD (τ_{PF}) at wavelength 440 nm for the 17 AERONET sites for the timeframe from 2001–2018. The dashed lines show ordinary least square regression lines.

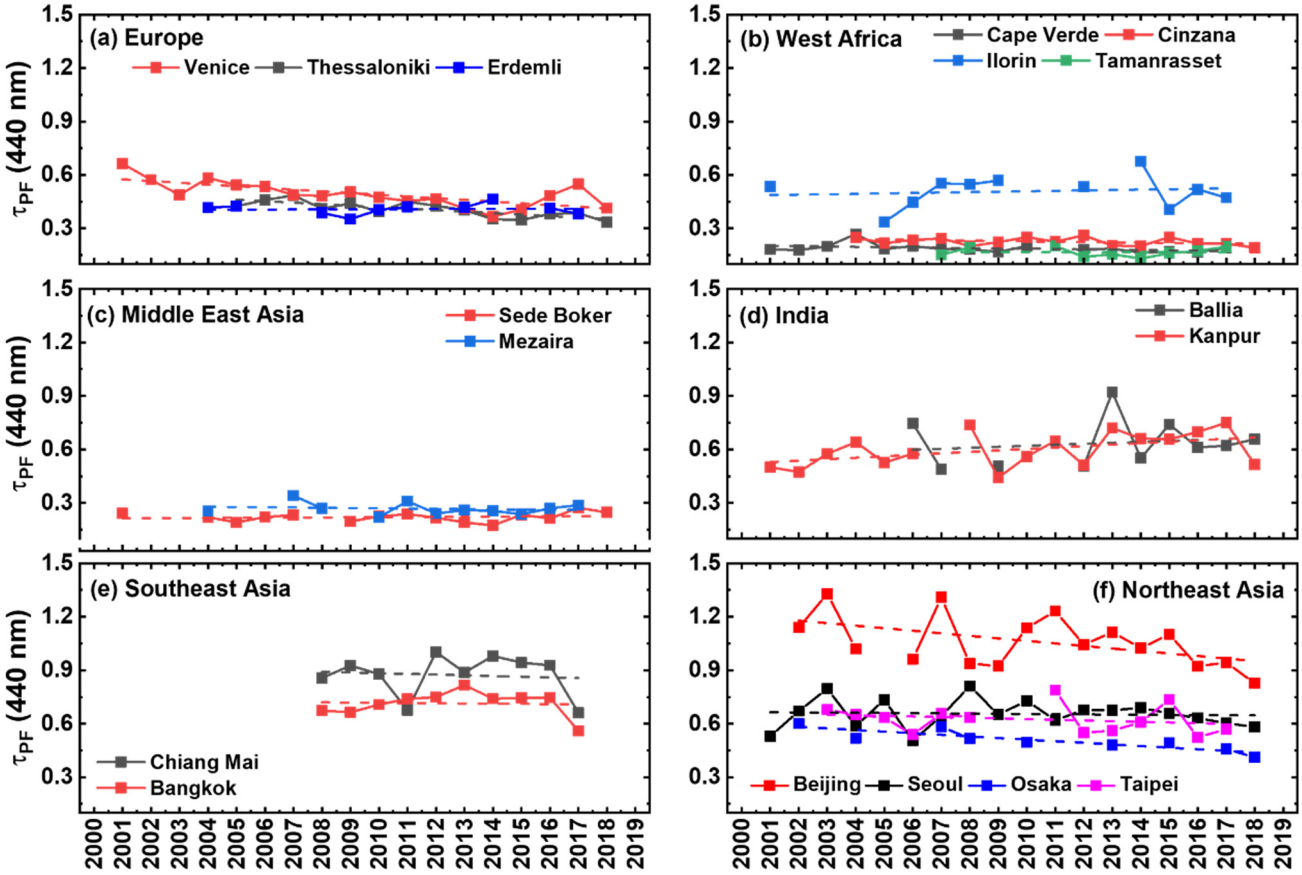

Figure S6. Annual trend of the total Ångström exponent (α_T) for the wavelength interval 440–870 nm for the 17 AERONET sites for the timeframe from 2001–2018. The dashed lines show ordinary least square regression lines.

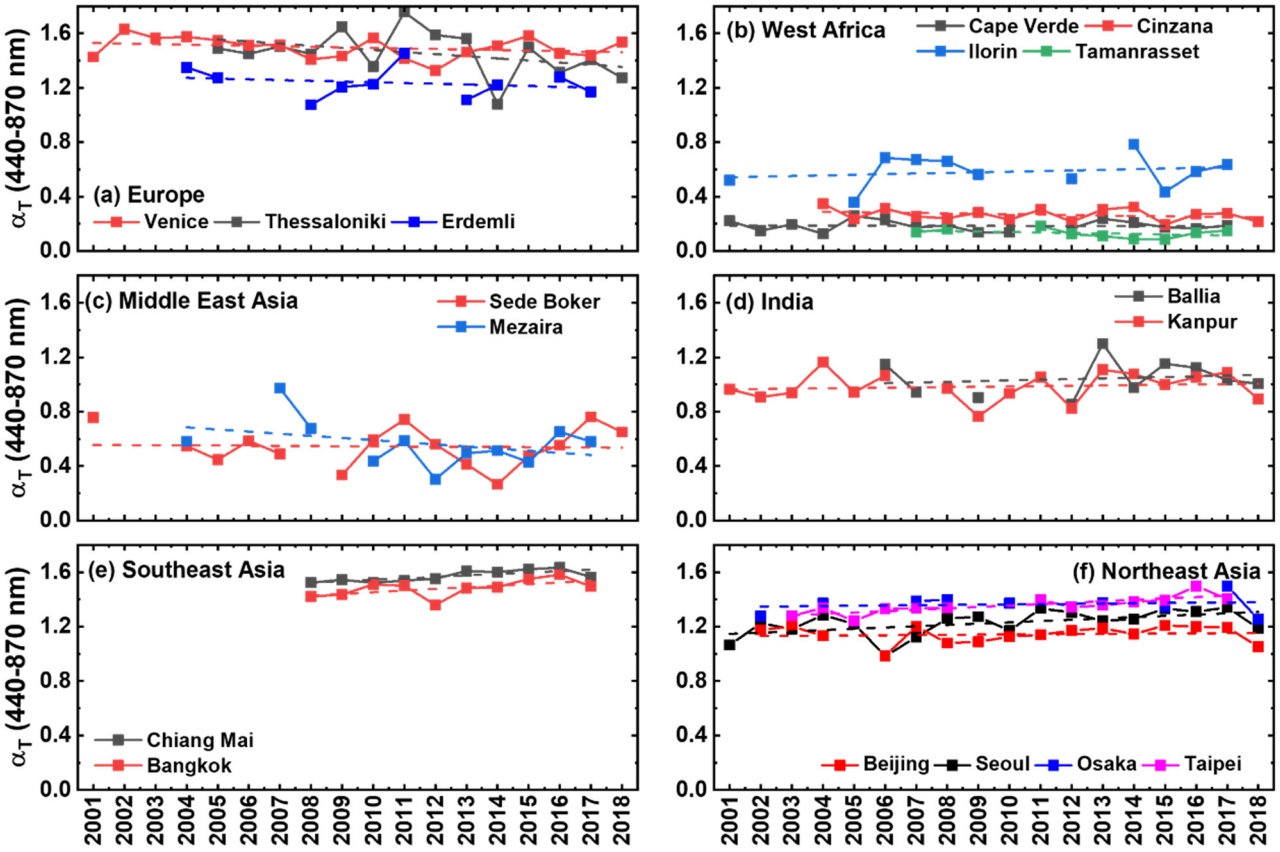

Figure S7. Annual trend of the Ångström exponent of fine-mode pollution particles (α_{PF}) for the wavelength interval 440–870 nm for the 17 AERONET sites for the timeframe from 2001–2018. The dashed lines show ordinary least square regression lines.

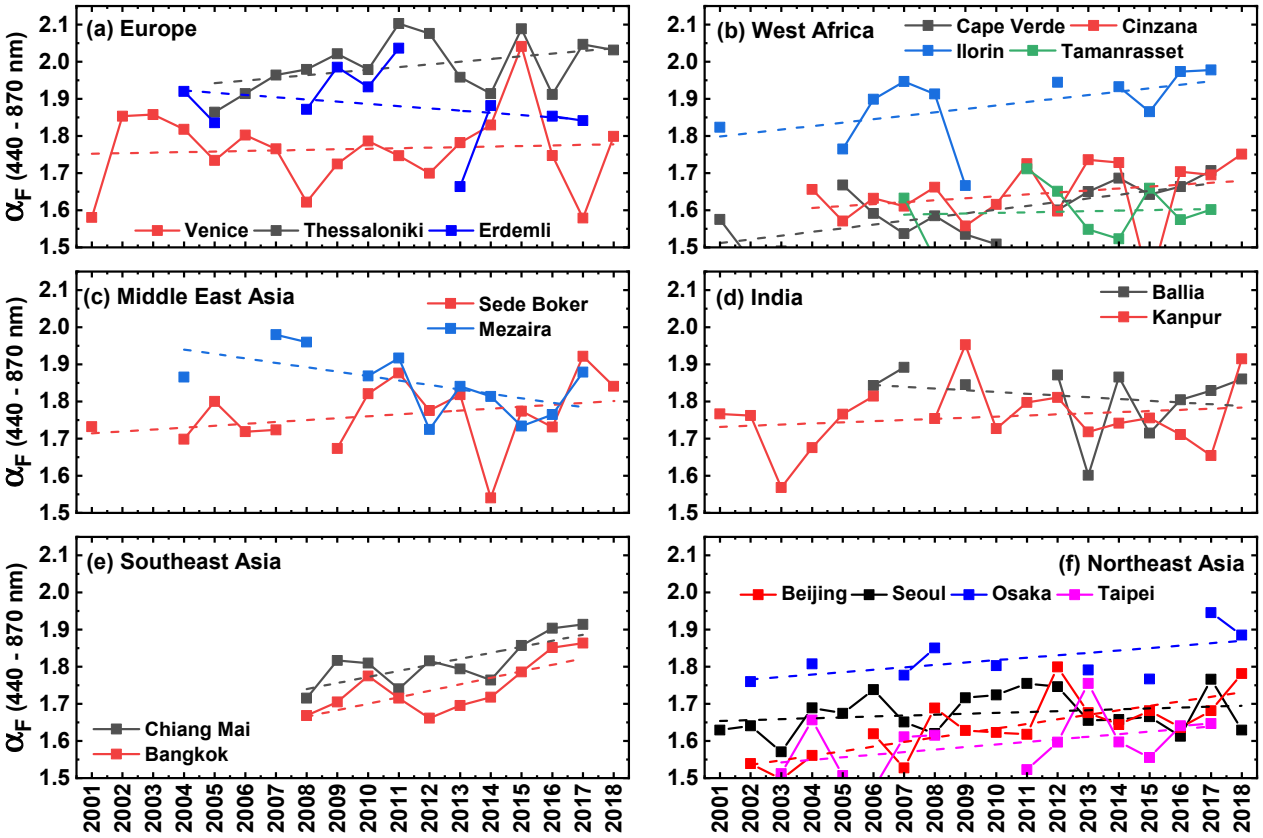

Region	Year / site	01	02	03	04	05	06	07	08	09	10	11	12	13	14	15	16	17	18	Total
Europe	Thessaloniki (40.63°N, 22.96°E)	-	-	-	-	25	63	31	36	45	42	56	30	34	9	27	24	20	23	**465**
	Venice (45.31°N, 12.51°E)	16	42	57	42	57	39	38	18	24	29	31	34	18	14	13	18	15	9	**514**
	Erdemli (36.56°N, 34.26°E)	4	-	-	43	51	-	-	71	41	34	50	-	13	31	-	44	18	-	**400**
North Africa	Cape Verde (16.73°N, 22.94°W)	60	34	55	24	53	39	56	50	27	35	-	40	27	35	43	47	25	13	**663**
	Cinzana (13.28°N, 5.93°W)	-	-	-	55	130	91	120	80	89	114	115	71	78	88	81	62	35	37	**1246**
	Ilorin (8.48°N, 4.67°E)	50	-	-	-	63	39	99	91	72	-	-	93	-	50	97	97	83	-	**834**
	Tamanrasset (22.79°N, 5.53°E)	-	-	-	-	-	-	38	57	-	-	44	39	40	47	36	49	47	-	**397**
Middle East Asia	Sede Boker (30.86°N,34.78°E)	11	-	-	25	19	28	16	-	14	42	33	31	23	16	33	27	41	26	**385**
	Mezaira (23.10°N, 53.75°E)	-	-	-	70	-	-	50	35	-	93	54	57	88	60	71	31	74	-	**683**
India	Ballia (25.87°N, 84.13°E)	-	-	-	-	-	104	62	-	99	-	-	135	27	101	113	91	61	88	**881**
	Kanpur (26.51°N, 80.23°E)	172	144	62	72	198	56	-	61	123	157	210	150	173	159	178	211	177	120	**2423**
Southeast Asia	Chiang Mai (18.77°N, 98.97°E)	-	-	-	-	-	-	-	82	89	126	72	59	97	85	82	60	57	-	**809**
	Bangkok (13.82°N, 100.04°E)	-	-	-	-	-	-	-	91	106	112	77	43	81	76	96	98	57	-	**837**
Northeast Asia	Beijing (39.98°N, 116.38°E)	-	71	81	67	-	87	60	27	68	96	71	42	40	71	56	73	46	63	**1019**
	Seoul (37.46°N, 126.95°E)	68	43	50	80	45	33	58	18	55	9	94	88	82	88	75	51	50	76	**1063**
	Osaka (34.65°N, 135.59°E)	-	21	-	39	-	-	39	32	-	32	-	-	46	-	36	-	21	26	**292**
	Taipei (25.02°N, 121.54°E)	-	7	25	15	27	8	47	-	-	14	18	12	17	26	37	13	23	-	**289**

Table S1. Number of observation days in each year for the 17 AERONET Sun/sky radiometer sites (version 3 level 2.0 data)